Elastic Fiber Fragmentation Increases Transmural Hydraulic Conductance and Solute Transport in Mouse Arteries

Austin J. Cocciolone
Department of Biomedical Engineering,
Washington University,
St. Louis, MO 63130

Elizabeth O. Johnson
Department of Mechanical Engineering and
Materials Science,
Washington University,
St. Louis, MO 63130

Jin-Yu Shao
Department of Biomedical Engineering,
Washington University,
St. Louis, MO 63130

Jessica E. Wagenseil[1]
Department of Mechanical Engineering and
Materials Science,
Washington University,
St. Louis, MO 63130
e-mail: jessica.wagenseil@wustl.edu

Transmural advective transport of solute and fluid was investigated in mouse carotid arteries with either a genetic knockout of fibulin-5 ($Fbln5^{-/-}$) or treatment with elastase to determine the influence of a disrupted elastic fiber matrix on wall transport properties. Fibulin-5 is an important director of elastic fiber assembly. Arteries from $Fbln5^{-/-}$ mice have a loose, noncontinuous elastic fiber network and were hypothesized to have reduced resistance to advective transport. Experiments were carried out ex vivo at physiological pressure and axial stretch. Hydraulic conductance (L_P) was measured to be $4.99 \times 10^{-6} \pm 8.94 \times 10^{-7}$, $3.18^{-5} \pm 1.13 \times 10^{-5}$ ($p < 0.01$), and $3.57 \times 10^{-5} \pm 1.77 \times 10^{-5}$ ($p < 0.01$) $mm{\cdot}s^{-1}{\cdot}mmHg^{-1}$ for wild-type, $Fbln5^{-/-}$, and elastase-treated carotids, respectively. Solute fluxes of 4, 70, and 150 kDa fluorescein isothiocyanate (FITC)-dextran were statistically increased in $Fbln5^{-/-}$ compared to wild-type by a factor of 4, 22, and 3, respectively. Similarly, elastase-treated carotids demonstrated a 27- and 13-fold increase in net solute flux of 70 and 150 kDa FITC-dextran, respectively, compared to untreated carotids, and 4 kDa FITC-dextran was unchanged between these groups. Solute uptake of 4 and 70 kDa FITC-dextran within $Fbln5^{-/-}$ carotids was decreased compared to wild-type for all investigated time points. These changes in transport properties of elastic fiber compromised arteries have important implications for the kinetics of biomolecules and pharmaceuticals in arterial tissue following elastic fiber degradation due to aging or vascular disease. [DOI: 10.1115/1.4042173]

Keywords: elastic fiber matrix, fibulin-5, porous membrane

Introduction

Targeted pharmacological intervention of vascular disease is an increasing area of research for the treatment of localized defects. The prevention of restenosis following the stenting of occluded arteries in coronary artery disease through the use of drug-eluting stents has proven efficacious [1–3] and similar drug eluting stent strategies are being considered for treating atherosclerotic peripheral arteries. Drug delivery strategies are in development to prevent neointimal hyperplasia following arterial reconstruction, grafting, and endarterectomy of the aorta and common carotids [4,5]. Pharmacological management of aortic aneurysms has shown promise in animal studies [6–9] but has been inconsistent clinically [10,11] and now targeted delivery of these drugs is being considered [12–16]. With this increasing focus on localized drug delivery to arterial tissues, the pharmokinetics of these tissues is of interest to better understand the physical forces that regulate the delivery and retention of the therapeutic agent within the targeted area [17]. In part, this includes characterization of the transport properties of arterial tissue and how these properties are affected by structure and composition of the arterial wall.

The wall of large elastic arteries is composed of three layers: intima, media, and adventitia. The intima is a single layer of endothelial cells that is directly adjacent to the lumen. The media is the middle layer and makes up the majority of the tissue in the arterial wall. The media is further sublayered into concentric layers composed of vascular smooth muscle cells (VSMCs) and an extracellular matrix (ECM) rich in collagen and elastic fibers. These sublayers are defined by dense sheets of elastic fibers called elastic lamellae that appear as concentric formations in the arterial wall. The outermost layer is the adventitia, composed of fibroblasts and a loose collagen-rich ECM [18–20].

The endothelial cell layer of the intima is regarded as the most important barrier to the transport of biological macromolecules and drugs supplied from blood in the lumen to reaching the innermost layers of the arterial wall [21–25]. Less attention has been given to mass transport beyond the intima. Many transport models and experiments tend to assume the media to be homogenous and the VSMCs to be the main obstacle to solute transport [23,25–28]. The large ECM component of the media and its unique layered structure attributed to the elastic lamellae are not appreciably considered by these models. Several numerical investigations account for ECM in arterial wall transport and provide evidence that ECM structure and composition are important contributors toward media layer effective porosity [25,29]. Hwang and Edelman observed anisotropic mass transport in bovine carotid tissue with diffusion in the circumferential direction being greater than diffusion in the transmural direction [30] and they proposed this may be a result of the nonhomogenous arrangement of the elastic fiber network.

These previous studies provide evidence of ECM contribution to transport within the arterial wall but none of them are able to isolate the role of individual ECM constituents. Due to its abundance in the wall and its concentric layering as thick sheets within the arterial media, we suspect that elastic fibers play a crucial role in limiting solute transport across the wall. To evaluate the role of elastic fibers in arterial wall transport, we performed transport studies in fibulin-5 null ($Fbln5^{-/-}$) mice. Fibulin-5 has the critical role in elastic fiber assembly of regulating and directing tropoelastin, the monomeric precursor, to mature polymeric elastic fibers. The elastic lamellae of $Fbln5^{-/-}$ arteries are fragmented and improperly organized [31,32] and we hypothesized that $Fbln5^{-/-}$ arteries have reduced resistance to transmural transport. We

[1]Corresponding author.

Manuscript received August 3, 2018; final manuscript received November 12, 2018; published online December 19, 2018. Assoc. Editor: Seungik Baek.

measured fluid and solute transport in $Fbln5^{+/+}$ and $Fbln5^{-/-}$ carotid arteries and observed an increase in the hydraulic conductance and solute flux in the elastic fiber compromised tissue. Additionally, we supplemented our findings from $Fbln5^{-/-}$ tissue by measuring transport across $Fbln5^{+/+}$ tissues following exposure to elastase, an enzyme with high affinity for elastic fibers, and found similar results.

Methods

Transport Theory. Here, we have approximated the arterial wall tissue to be a porous membrane with a homogenous distribution of uniformly shaped, cylindrical pores. Movement of solute molecules across any porous membrane occurs through a combination of diffusive and advective (bulk flow) transport mechanisms. In a sieving membrane, solvent molecules pass unhindered across the membrane while the solute molecules experience some degree of difficulty in transport. Steric exclusion based on the size of the solute and pore contributes to preventing the solute from entering the membrane. Additionally, the traveling velocity of the solute within the pore may be reduced by hydrodynamic interaction between the pore wall and the solute.

The differential form of the advection-diffusion equation for one-dimensional, steady-state solute transport is given as follows:

$$J_s = (1-\sigma)J_v c - D_s \frac{dc}{dx} \tag{1}$$

where J_s is the net solute flux across the membrane, J_v is the volumetric fluid flux, D_s is an effective diffusivity coefficient of the solute within the membrane, c is the solute concentration in the membrane at some distance x, and σ is the osmotic reflective coefficient which is used to express the fraction of molecules that are reflected back instead of entering the membrane [33].

An expression for J_v can be derived from D'Arcy's law

$$J_v = \frac{\dot{Q}_f}{A_m} = \frac{\kappa}{\mu}\left(\frac{dP}{dx} - \sigma RT\frac{dc}{dx}\right) \tag{2}$$

where $\dot{Q}_f$ is the volumetric flowrate, A_m is the cross-sectional area of the membrane normal to the flow, κ is the intrinsic permeability, μ is the dynamic fluid viscosity, P is the hydrostatic pressure, R is the gas constant, and T is the temperature.

Equations (1) and (2) were derived by Kedem and Katchalsky [33] to describe solute transport of a neutral solute across a thin, homogenous porous membrane permeable to both solute and solvent. Integration of Eq. (1) across the thickness of the membrane yields

$$J_s = (1-\sigma)J_v \cdot g(c) - \frac{D_s}{\Delta x}\Delta c \tag{3}$$

where $g(c)$ is a function of solute concentration across the membrane. Likewise, integration of Eq. (2) yields

$$J_v = L_p(\Delta P - \sigma RT\Delta c) \tag{4}$$

where L_P is the hydraulic conductance, an intrinsic property that describes how easily water can move across the membrane.

$$L_p = \frac{\kappa}{\mu\Delta x} \tag{5}$$

L_p can be determined experimentally by measuring the volumetric fluid flux across a membrane at steady-state, constant pressure, and in absence of a solute concentration gradient. In which case Eq. (4) can be reduced and rearranged to

$$L_p = \frac{J_v}{\Delta P} \tag{6}$$

Animal Tissue Preparation. Intact common carotid arteries were removed from four-month-old (±14 days) $Fbln5^{+/+}$ and $Fbln5^{-/-}$ mice [34] euthanized by carbon dioxide inhalation in compliance with the Institutional Animal Care and Use Committee. The tissue was stored at 4 °C in phosphate-buffered saline (PBS) until testing which generally occurred within three days of dissection. Overall 92 mice were used in this study. Structural and mechanical properties of $Fbln5^{+/+}$ and $Fbln5^{-/-}$ carotids were investigated by Ferruzzi et al. and determined to be gender independent [35]. As a result, samples from this study were not separated by gender.

Experimental Setup. Mass transport experiments were conducted ex vivo using a pressure myograph testing system and the corresponding software (Danish Myo Technology, Copenhagen, Denmark). For each experiment, the ends of the carotid were cannulated and gently secured in-place using 7-0 suture and placed in a 10 mL PBS bath maintained at 37 °C. The carotid was then stretched to a stretch ratio of 1.4, which is the average in vivo stretch ratio for a mouse carotid artery [36]. Denudation of the endothelium was achieved by bubbling 20 mL of air through the lumen at a constant rate [37]. During this step, the integrity of the artery was confirmed by clamping the outlet tubing and pressurizing the carotid with air to 100 mmHg. Air escaping from the lumen to the bath indicated a hole in the tissue and the experiment was not performed. Intact carotids were then pressurized to a hydrostatic pressure of 100 mmHg using a fluid column attached to the myograph inlet and clamping the tubing at the myograph outlet. One of three experimental procedures was performed for the measurement of volumetric fluid flux, net solute flux, or solute uptake into the media. These experiments were performed on carotids from $Fbln5^{+/+}$ and $Fbln5^{-/-}$ mice as well as carotids from $Fbln5^{+/+}$ mice after an elastase treatment.

Elastase Treatment. After mounting and stretching the carotid but before inflation with the hydrostatic pressure column, $Fbln5^{+/+}$ carotids were subjected to an elastase treatment. 7.5 units/mL elastase (EC134, Elastin Products Co., Owensville, MO) was introduced into the lumen of the artery by a syringe through the inlet tubing. The outlet tubing was clamped and the artery was pressurized and held at 100 mmHg by further depressing the syringe. After 30 s, elastase activity was inhibited by submerging the mounted carotid in a bath containing a stop solution of 100 mM NaCl PBS [38] and the lumen of the carotid was flushed with the same solution. The carotid was pressurized to 100 mmHg and was maintained submerged in stop solution for 30 min. The lumen was then flushed with regular PBS and the bath was replaced with 10 mL of fresh PBS and the carotid was ready for experimentation. Effectiveness of the elastase treatment and subsequent inhibition was verified in a pilot study by tracking post-treatment diameter of the carotid. Uninhibited elastase-treated carotids continued to increase in diameter during the 1 h observation period while the inhibited elastase-treated carotids held a constant diameter (data not shown). An increase of 15.6% (±5.6%) in outer diameter was observed in the elastase-treated carotids used in this study.

Hydraulic Conductance. A modification was made to the experimental setup to include a length of tubing between the myograph inlet and the pressure fluid column. Using a syringe and three-way stopcock, an air bubble was added to this tubing. After preparing the artery for testing, displacement of the bubble was measured by taking an image every 2 min for 60 min. By continuity, the volumetric flowrate of the fluid in the tubing is equivalent to the transmural volumetric flowrate across the arterial wall leading to the following relation:

$$Q = A \cdot \overline{V} = A_A \cdot \left.\frac{dx}{dt}\right|_A = A_T \cdot \left.\frac{dx}{dt}\right|_T \tag{7}$$

where Q is the fluid volumetric flowrate,A is the cross-sectional area normal to flow and $\overline{V}$ is the mean fluid velocity for the artery ($_A$) and tubing ($_T$). Equation (7) can be rearranged to express the transmural fluid flux across the artery (J_v) and expanding the area in terms of diameter and suture-to-suture length for the artery and inner diameter of the tubing (d_A, $l_{A,S}$, and d_T, respectively).

$$J_v = \frac{Q}{A_A} = \frac{{d_T}^2 \cdot \frac{\Delta x_{\text{bubble}}}{\Delta t}}{4 \cdot d_A \cdot l_{A,S}} \tag{8}$$

At steady-state, the volumetric fluid flux can be determined from the slope of displacement versus time curve for the air bubble and Eq. (8). Further, hydraulic conductance can be calculated using this fluid flux and Eq. (6) in the solute-free case where the reflection coefficient is zero.

Solute Flux. Net solute transport was assessed by adding 2.5 mg/mL of 4, 70, or 150 kDa fluorescein isothiocyanate (FITC)-dextran (Sigma-Aldrich Co., St. Louis, MO; #46944, #46946, and #46946, respectively) to the fluid column such that the lumen of the carotid contained a molar concentration of 625, 35.7, or 16.7 μM FITC-dextran, respectively. Transmural solute transport was monitored over 60 min by sampling 50 μL from the fluid bath outside of the artery twice every 10 min after mixing. Concentration was determined fluorometrically (480 nm excitation, 525 nm emission) against a serial dilution of the 2.5 mg/mL stock solution using a plate reader (SpectraMax M2^e, Molecular Devices, San Jose, CA). Net solute flux, J_s, was calculated by the following equation:

$$J_s = \frac{1}{A_A} \cdot \frac{\Delta c_{\text{bath}}}{\Delta t} \tag{9}$$

where $\Delta c_{\text{bath}}/\Delta t$ is the slope of the bath concentration versus time curve at steady-state.

Solute Uptake. Similar to the solute flux experiments, 2.5 mg/mL of 4, 70, or 150 kDa FITC-dextran was added to the fluid column. Transmural advective transport persisted for 30, 60, 120, or 240 min in the 4 kDa and 70 kDa experiments but only the 60 min time point was taken for the 150 kDa experiments. Postexperiment, the arterial lumen was flushed with solute-free PBS. The artery was removed from the myograph by cutting each end at the tip of the cannulae. A lateral cut was made the length of the artery to expose the lumen to facilitate the elution of FITC-dextran from the tissue. A series of elutions was performed by placing the artery in a vial containing 120 μL of PBS and placing the vial on a shaker at 300 rpm and 37 °C, transferring the tissue to a fresh vial every 24 h. In total, the artery underwent three elutions and the fluorescence of each elutant was measured and compared to a standard curve generated from a serial dilution of stock 2.5 mg/mL FITC-dextran that had undergone the same conditioning as the samples. Typically, 80% of the eluted FITC-dextran appeared in the first elution and the final elution contained less than 5% of the sum between the three elutions providing confidence that the majority of FITC-dextran taken up by the artery during the experiment had been eluted. The values reported are not a true concentration since arterial wall thickness was not measured, however it has been previously determined that wall thickness is similar between $Fbln5^{+/+}$ and $Fbln5^{-/-}$ arteries [32,36]. Therefore, solute uptake is reported here as the total number of moles of FITC-dextran taken up by the wall normalized to the artery length in the experiment (i.e., μmol FITC-dextran·mm^{-1}).

Histology. Four each of $Fbln5^{+/+}$, $Fbln5^{-/-}$, and elastase-treated $Fbln5^{+/+}$ carotids were fixed in 10% formaldehyde for 24 h followed by dehydration in ethanol. The samples were paraffin embedded and sectioned at the Musculoskeletal Histology and Morphometry Core at the Washington University School of Medicine. Verhoeff Van Gieson (VVG) stain was used for visualization of the elastic fiber network structure within the cross section of the carotid wall. Qualitative assessment of the integrity of the elastic lamellae was compared across the three groups.

Two-Photon Microscopy. Immediately following dissection and elastase treatment, if required, four each of $Fbln5^{+/+}$, $Fbln5^{-/-}$, and elastase-treated $Fbln5^{+/+}$ carotids were fixed for one hour in 4% paraformaldehyde at 4 °C. *En face* slides were prepared by performing a lateral cut the length of the artery and mounting the tissue on the slide such that the lumen faced upward and in direct contact with the coverslip. Imaging was performed by the Washington University Center for Cellular Imaging (WUCCI) at the Washington University School of Medicine using a Zeiss LSM 880 Airyscan two-photon microscope and a 40×/1.2 silicon immersion objective. A z-stack of elastin auto fluorescence was captured at 330 nm increments across the thickness of the arterial wall by using a 488 nm laser for excitation and collecting the emission signal between 500 nm and 550 nm [39,40]. Deconvolution of the z-stacks was performed using the software, AUTOQUANT.

Statistics. Comparisons were made between tissue types at the same FITC-dextran size or time point. All statistics were performed using GRAPHPAD PRISM software with significance considered at $P < 0.05$. All comparisons were performed by a one-way ANOVA and Tukey's posthoc. Statistical significance between $Fbln5^{+/+}$ and $Fbln5^{-/-}$ (*), $Fbln5^{+/+}$ and elastase-treated $Fbln5^{+/+}$ (†), and $Fbln5^{+/+}$ and elastase-treated $Fbln5^{+/+}$ (#) samples are indicated on the figures.

Results

Histology. Representative VVG stains of $Fbln5^{+/+}$, $Fbln5^{-/-}$, and elastase-treated $Fbln5^{+/+}$ carotid cross section are presented in Fig. 1. The elastic lamellae (stained in black) from the $Fbln5^{+/+}$ (1(*a*)) appear as smooth, continuous layers within the media. In contrast, the continuity of the elastic lamellae in the $Fbln5^{-/-}$ tissue (1(*b*)) is disrupted by over-deposition of elastin in some areas and under-deposition in others lending to an overall fragmented appearance. These histological images are in agreement with previously published results [31,32,34]. The elastase-treated $Fbln5^{+/+}$ carotid (1(*c*)) retains the continuity of the elastic lamellae and the elastic lamellae appear to be thinner than in untreated $Fbln5^{+/+}$. The elastase treatment used in this study was intended to reduce the transport resistance of the elastic lamellae but to avoid complete removal of the elastic fibers and the histology images indicate that the elastic lamellae are still intact. The surrounding VSMCs appear more loosely arranged than in the $Fbln5^{+/+}$ tissue, possibly due to the removal of the thin elastic fibers in the muscle tissue regions between elastic lamellae.

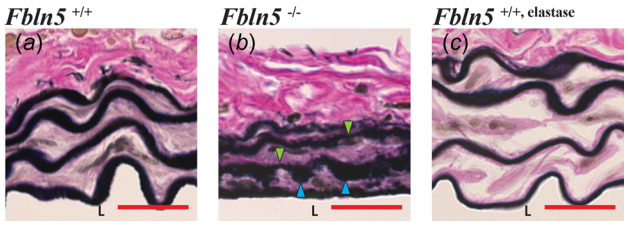

Fig. 1 Representative histological cross section of *Fbln5*$^{+/+}$ (*a*), *Fbln5*$^{-/-}$ (*b*), and elastase-treated *Fbln5*$^{+/+}$ (*c*) carotid arteries. The elastic lamellae are colored black by the VVG stain. The arterial lumen (L) is toward the bottom of the images. Phenotypic over-deposition and under-deposition of elastin within the elastic lamellae of *Fbln5*$^{-/-}$ are indicated by blue, upward-facing arrows and green, downward-facing arrows, respectively. The scale bar indicates 20 μm. Please see online version for color images.

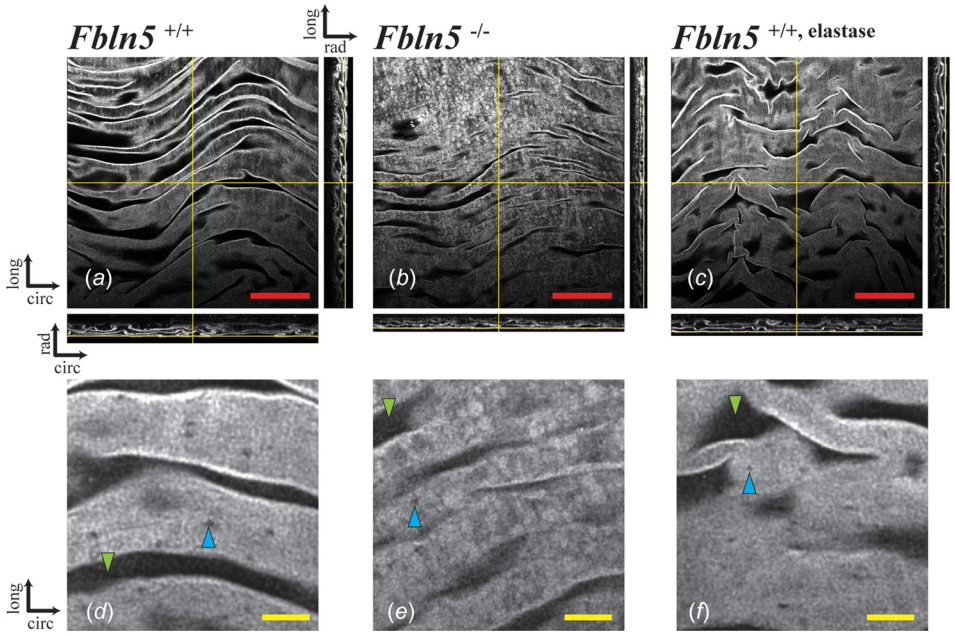

Fig. 2 Representative two-photon microscopy images of elastin auto fluorescence from *en face* $Fbln5^{+/+}$ (*a* and *d*), $Fbln5^{-/-}$ (*b* and *e*), and elastase-treated $Fbln5^{+/+}$ ((*c*) and (*f*)) carotids. Panels (*a*, *b*, and *c*) are views of a single plane from the z-stack within the internal elastic lamella. Orthogonal views of the z-stack are shown next to Panels *a*, *b*, and *c* for three-dimensional visualization. The orientation for each image is indicated (circ = circumferential, long = longitudinal, rad = radial). The yellow lines represent the image location within the z-stack. The red scale bar (top) indicates 50 μm. Panels *d*, *e*, and *f* are magnified z-projections of four consecutive planes from the z-stack within the internal elastic lamella. Blue, upward facing arrows indicate a fenestration (hole) within the elastic lamina. Green, downward facing arrows show the elastic lamella undulating out of the z-projection plane. The yellow scale bar (bottom) indicates 10 μm. Please see online version for color images.

Two-Photon Microscopy. Representative *en face* images from the two-photon microscopy of elastin auto fluorescence from $Fbln5^{+/+}$, $Fbln5^{-/-}$, and elastase-treated $Fbln5^{+/+}$ carotids are shown in Fig. 2. A single plane of the en face z-stack and the orthogonal views are shown to visualize the elastic fiber network in three-dimensions. The elastic lamellae undulate in-and-out of the en face image plane as a result of their characteristic wavy pattern, which is evident from the orthogonal views and the histological cross section in Fig. 1. The over- and under-deposition of elastin within the lamellae of $Fbln5^{-/-}$ arteries is evident in the en face images and is consistent with the histological images. Changes in the density and arrangement of the elastic fibers may increase the effective porosity of the $Fbln5^{-/-}$ elastic lamellae and contribute to the observed increase in solute transport. Fenestrations (holes) in the elastic lamellae are visible in the higher magnification en face images and appear similar in all three groups. There is no apparent difference in elastic fiber density or organization due to the elastase treatment, indicating the subtle nature of the treatment protocol. Additional more quantitative investigation is required to identify structural changes in the elastase treated group that may contribute to the observed differences in transport properties.

Hydraulic Conductance. Steady-state volumetric fluid flux was achieved rapidly after the start of the experiment, evidenced by the linear displacement curves of the tracking bubble (Fig. 3(*a*), $R^2 > 0.99$ in all experiments). The slope of the displacement curve was used in Eq. (8) to determine volumetric fluid flux, which was then used with Eq. (6) to calculate the intrinsic hydraulic conductance for each group (Fig. 3(*b*)). The elastic fiber compromised tissue of the $Fbln5^{-/-}$ and elastase-treated $Fbln5^{+/+}$ carotids resulted in a six- and sevenfold increase in hydraulic conductance, respectively, compared to $Fbln5^{+/+}$ tissue.

Solute Flux. It is apparent by the constant rate of change in FITC-dextran concentration in the external bath that the solute transport across the arterial wall reached steady-state in less than 10 min of experimentation for all tested FITC-dextran sizes (Figs. 4(*a*)–4(*c*), $R^2 > 0.98$ in all experiments). The slope of the bath concentration versus time curves and Eq. (9) was used to determine the net solute flux across the wall (Fig. 4(*d*)). $Fbln5^{-/-}$ carotids have a fourfold increase in 4 kDa FITC-dextran solute flux compared to $Fbln5^{+/+}$ carotids. The change in solute flux is more drastic in the case of 70 kDa, having a 22-fold increase in $Fbln5^{-/-}$ compared to $Fbln5^{+/+}$. However, in the case of 150 kDa the difference drops to a threefold increase. Overall, the $Fbln5^{-/-}$ tissue exhibits a linear decrease in solute flux with increasing dextran size on the semilog scale (Fig. 4(*d*)) while the $Fbln5^{+/+}$ tissue experiences a sharper decrease in solute flux from 4 kDa to 70 kDa but a minimal change in solute flux from 70 kDa to 150 kDa. This indicates a shift in the size exclusion limit between the tissues as a result of the elastic fiber fragmentation in the $Fbln5^{-/-}$ tissue.

Elastase-treated $Fbln5^{+/+}$ carotids have a 4 kDa solute flux that is not significantly different from untreated tissue (Fig. 4(*d*)). There is a significant increase in 70 kDa solute flux and it is comparable in magnitude to the increase demonstrated by $Fbln5^{-/-}$ carotids over untreated $Fbln5^{+/+}$ carotids at the same dextran size. The 150 kDa solute flux in elastase-treated $Fbln5^{+/+}$ carotids is significantly increased 13-fold and fourfold over $Fbln5^{+/+}$ and $Fbln5^{-/-}$ carotids, respectively. The net solute flux of FITC-dextran across elastase-treated tissue is independent of dextran size, suggesting that the relative pore size is increased sufficiently that the tissue no longer has sieving capability at the tested FITC-dextran sizes. The results for the elastase-treated tissue provide additional evidence that changes to the elastic fiber network structure will alter solute transport. Based on the

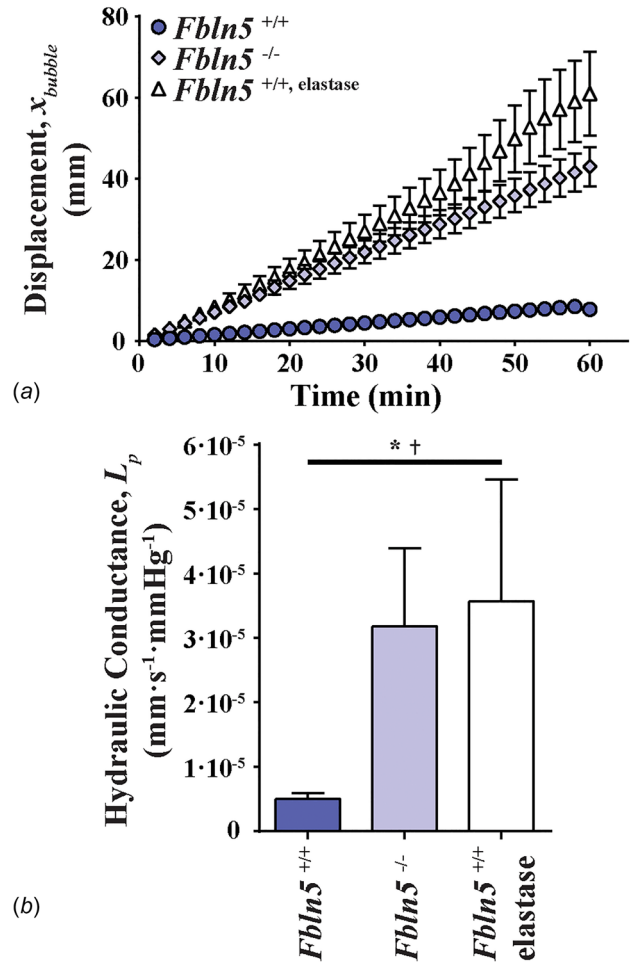

Fig. 3 Results from the volumetric fluid flux experiments. Panel *a*—the displacement of the tracking bubble over time for each of the tissues. Error bars are standard error of the mean (SEM) for clarity. Panel *b*—hydraulic conductance of $Fbln5^{+/+}$ ($n = 7$), $Fbln5^{-/-}$ ($n = 8$), and elastase-treated $Fbln5^{+/+}$ carotids ($n = 8$). Error bars are SD. Statistical significance was determined between $Fbln5^{+/+}$ and $Fbln5^{-/-}$ (*$p = 0.0021$) and between $Fbln5^{+/+}$ and elastase-treated $Fbln5^{+/+}$ (†$p = 0.0004$).

differences in behavior between the groups for different FITC-dextran sizes, it appears that alterations in solute transport depend on the mechanisms leading to elastic fiber defects (i.e., genetic disruptions in elastic fiber assembly versus protease digestion of mature elastic fibers).

Solute Uptake. Dextran uptake concentration was decreased in the $Fbln5^{-/-}$ tissue compared to $Fbln5^{+/+}$ for 4–70 kDa FITC-dextran at every time point tested (Figs. 5(*a*) and 5(*b*), respectively). In these time course experiments, there was a steady increase in solute uptake over time. This may be a result of passive diffusion of solute into void spaces within the tissue that are not accessible to the transmural fluid flux.

The 4 kDa FITC-dextran concentration (Fig. 5(*a*)) was increased in both $Fbln5^{+/+}$ and $Fbln5^{-/-}$ carotids compared to 70 kDa FITC-dextran (Fig. 5(*b*)) at all time points and is likely a result of a combination of factors including the larger molar concentration and smaller solute size of 4 kDa FITC-dextran.

Solute uptake for 150 kDa FITC-dextran was measured only after 60 min. A comparison of solute uptake for each dextran size at 60 min is presented in Fig. 5(*c*). Interestingly, the significant decrease in solute uptake by $Fbln5^{-/-}$ carotids in the 4–70 kDa studies is lost in the 150 kDa study. This indicates that 150 kDa FITC-dextran is large enough to minimize any impact of the differences in porosity between the $Fbln5^{+/+}$ and $Fbln5^{-/-}$ tissues

Additionally, solute uptake at each dextran size was measured after 60 min for elastase-treated $Fbln5^{+/+}$ arteries. The results are included in Fig. 5(*c*). At the 4 kDa FITC-dextran size, there is a decrease in solute uptake for elastase-treated $Fbln5^{+/+}$ arteries, comparable to that observed in the $Fbln5^{-/-}$ tissues. At 70 kDa, the behavior between these groups diverges as the elastase-treated tissue now has increased solute uptake compared to untreated tissue. The same trend is observed at 150 kDa FITC-dextran. Overall, the trend of reduced solute uptake observed with dextran size in $Fbln5^{+/+}$ and $Fbln5^{-/-}$ tissues is diminished in the elastase-treated tissues.

Discussion

To the best of our knowledge, this is the first empirical investigation of mass transport in the medial layer of arterial tissue in which the elastic fiber network has been specifically compromised. We have continued the assumptions made in other investigations that the media behaves as a homogenous, porous membrane to simplify experimentation and numerical analyses. Our investigation isolates the role of the elastic fiber network on the intrinsic transport properties of the arterial wall by comparing mass transport in wild-type mouse common carotids to those with genetically and enzymatically compromised elastic fiber integrity. While our investigation is focused on the elastic fibers, there are additional ECM components in the wall, including collagen fibers and proteoglycans, which may also influence arterial wall transport. Our observations of increased volumetric fluid flux and net solute flux in elastic fiber compromised tissues provide evidence that the ECM should not be overlooked in theoretical or experimental studies of arterial wall mass transport.

The hydrodynamic radius of 4, 70, and 150 kDa FITC-dextran is approximately 1.5, 5.9, and 8.6 nm, respectively [41]. These sizes are several orders of magnitude smaller than the radius (0.5–5 μm) of the fenestrae that are characteristic of the morphology of elastic lamellae within the arterial wall [42,43] and can be observed in the two-photon microscopy images presented in Fig. 2. The fenestrations implicitly contribute to the transmural hydraulic conductance of the arterial wall. However, their relatively large size suggests they are not a factor toward the resistance of solute transport of the dextran molecules used in this study. Increased size and frequency of fenestrations within the aorta have been observed in a mouse model of Marfan syndrome, an autosomal dominant genetic disorder having numerous connective tissue defects including elastic fiber fragmentation and dilation of the aorta [42]. Although the size and density of elastic lamellae fenestrations were not qualitatively different between groups in our study, additional quantitative analyses may highlight subtle differences that should be considered for transport of targeted pharmacologic therapies in elastic fiber related diseases, such as Marfan syndrome.

The effective radius of the pores passing between the elastic fibers within the elastic lamellae of wild-type arteries can be approximated to be between the hydrodynamic radii of 4–70 kDa FITC-dextran, based on the size exclusion behavior observed in Fig. 4(*d*). This size exclusion behavior is diminished in the $Fbln5^{-/-}$ artery, indicating a change in the effective pore radius of the genetic mutant and is likely a result of the apparent change in the density and arrangement of the elastic fibers within the elastic lamellae, as indicated in the two-photon microscopy images. The elastase-treated wild-type arteries allowed all sizes of FITC-dextran particles through at approximately the same rate. The size range at which these solute exclusion behaviors occur, or the absence of size exclusion behaviors, has important physiological implications on which biomolecules can more readily transverse the arterial wall. Cofactors and small molecule pharmaceuticals are generally smaller than 1 kDa and therefore may experience low resistance to transport by the elastic lamellae in wild-type

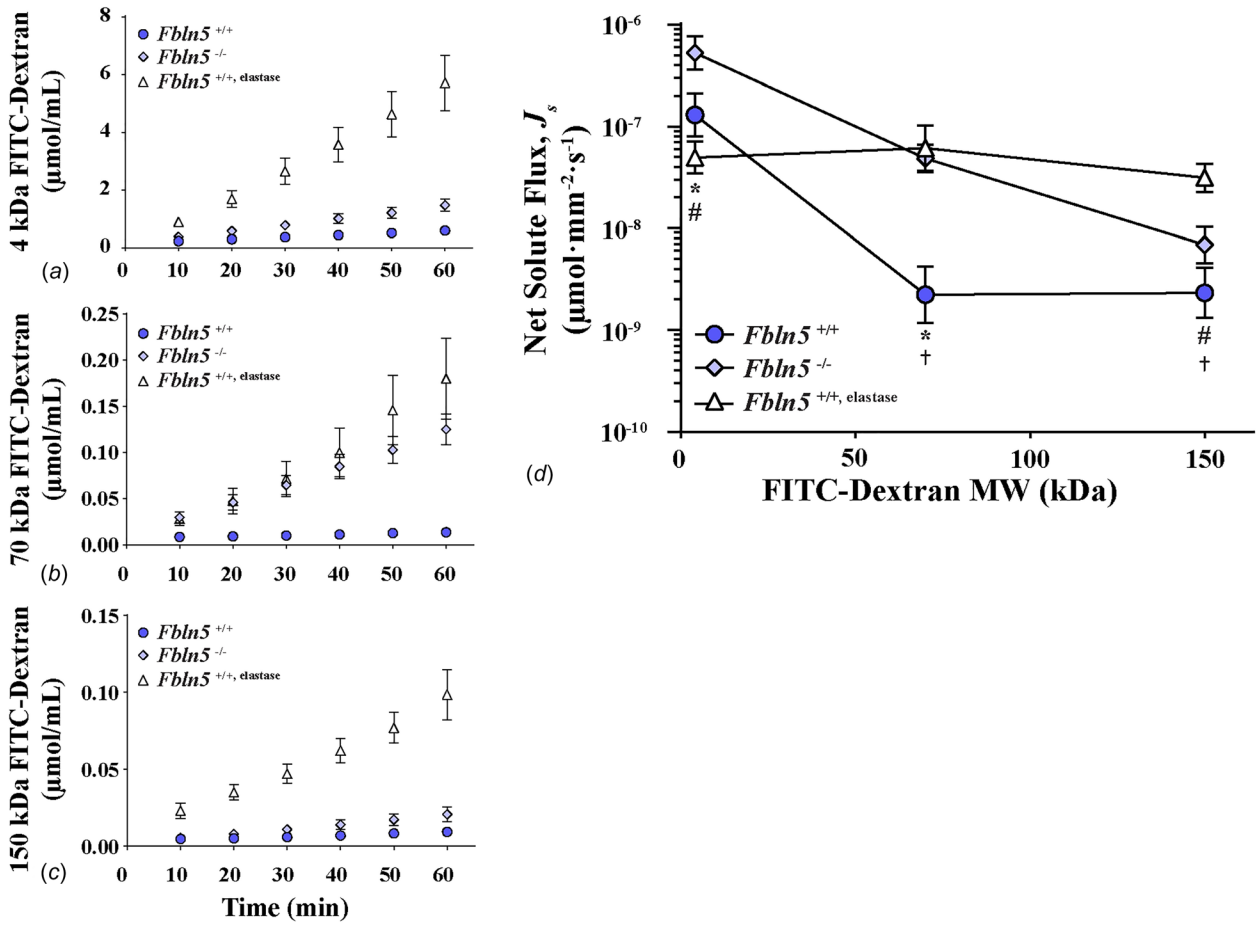

Fig. 4 Results from the net solute flux experiments. The change in solute concentration in the external bath with time for the 4, 70, and 150 kDa FITC-dextrans are shown in panels *a*, *b*, and *c*, respectively ($n = 5–9$). Error bars are SEM for clarity. Panel *d*—the net solute flux across the carotid wall of the investigated dextran sizes on a semilog plot. Statistical significance between *Fbln5*$^{+/+}$ and *Fbln5*$^{-/-}$ (*), *Fbln5*$^{+/+}$ and elastase-treated *Fbln5*$^{+/+}$ (†), and *Fbln5*$^{+/+}$ and elastase-treated *Fbln5*$^{+/+}$ (#) are indicated. Error bars are SD.

arteries. Biologics and growth factors which can span 10–100 kDa in size are likely impacted by the filtration effect of the elastic lamellae in wild-type arteries, but would more easily transverse the wall of arteries with genetic or enzymatic defects in the elastic lamellae. The elastic lamellae in wild-type arteries may be impermeable to much larger macromolecules such as members of the low-density lipoprotein family, which have significant contribution to the onset and progression of atherosclerosis, but may be permeable to these molecules when the elastic lamellae are enzymatically compromised.

Removal of the intimal layer of endothelial cells prior to experimentation allowed more direct measurement of medial layer transport properties, which has a prominent ECM component. The effect of stripping the endothelial layer on the hydraulic conductance of large elastic arteries has been studied previously by other investigators in order to isolate the medial layer contribution to transport. A denuded artery has a hydraulic conductance of nearly twice that of an intact vessel [44–46]. Our investigation further advances the knowledge of how arterial wall structural features contribute to advective transport resistance by demonstrating a sixfold and sevenfold increase in hydraulic conductance in *Fbln5*$^{-/-}$ and elastase-treated *Fbln5*$^{+/+}$ carotids, respectively, compared to untreated *Fbln5*$^{+/+}$. This increase in hydraulic conductance in the medial layer of elastic fiber compromised artery is strong evidence that the elastic fiber network contributes to the resistance of flow across the arterial wall.

Our investigation appears to be the first to report hydraulic conductance for mouse arterial tissue. Our wild-type arterial hydraulic conductance for the denuded mouse carotid is 49.9×10^{-8} cm·s^{-1}·mmHg^{-1} which is 5–40 times greater than values reported from studies involving arteries from other organisms. Performing transport experiments on mouse carotids is challenging owing to their small size. As such, the possibility that our results are overestimated due to an unforeseen technical limitation cannot be dismissed. However, there are several physiological differences in the elastic fiber network of mouse carotids compared to the arteries tested by other investigators that could account for this difference. The number of elastic lamellae tends to increase across animal species when ordered by animal size [47]. Additionally, the number of elastic lamellae within the media decreases along the arterial tree. We surmise these characteristics of the elastic fiber network structure could account for the differences. Hwang et al. observed differences in transport properties of arteries from different locations in the arterial tree [30]. Shou et al. reported a hydraulic conductance of 4.89×10^{-8} cm·s^{-1}·mmHg^{-1} at 100 mmHg for denuded rat aorta (eight lamellae) which has several more elastic lamellae than our mouse carotid (four lamellae) [47]; however, one caveat is that they did not apply an axial stretch to bring the artery to a physiological conformation for experimentation [46]. For the denuded rabbit aorta (~22 elastic lamellae), Tedgui and Lever report a hydraulic conductance at 180 mmHg of 5.27×10^{-8} cm·s^{-1}·mmHg^{-1} [44] and Baldwin et al. report a value of 3.5×10^{-8} cm·s^{-1}·mmHg^{-1} in one investigation [48] and 10.0×10^{-8} cm·s^{-1}·mmHg^{-1} in another investigation at 100 mmHg [45]. Tarbell et al. reported a value for the denuded rabbit carotid of 1.25×10^{-8} cm·s^{-1}·mmHg^{-1} at 100mHg which has ~6 more elastic lamellae than the mouse carotid [49–51].

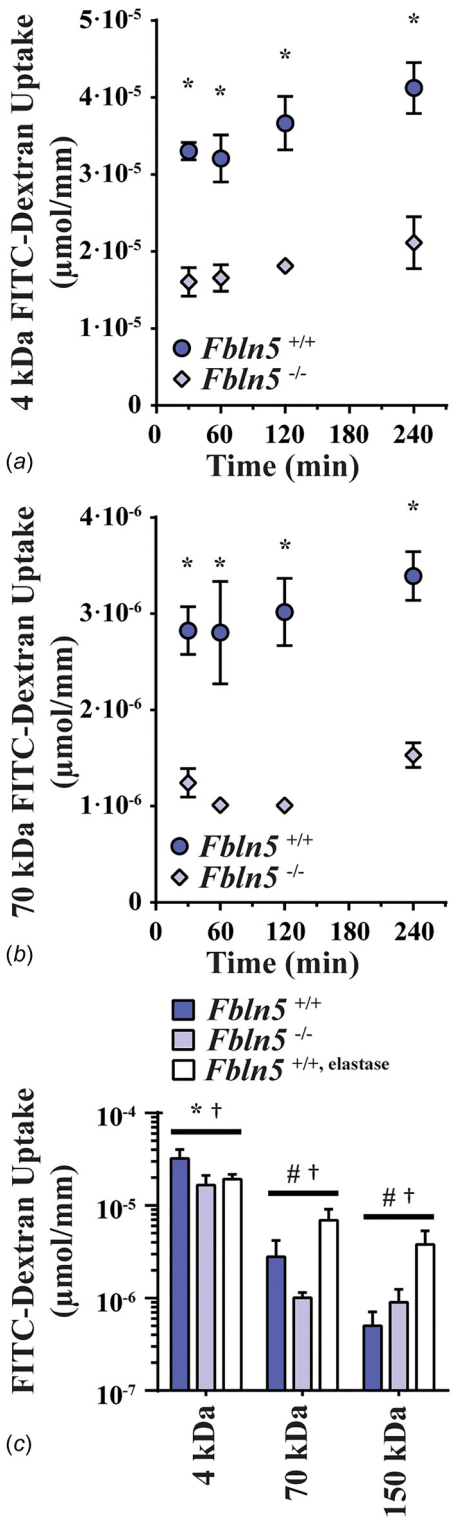

Fig. 5 Results from the solute uptake experiments. Quantity of 4 kDa (*a*) and 70 kDa (*b*) FITC-dextran retained within the wall of the $Fbln5^{+/+}$ and $Fbln5^{-/-}$ carotids after 30, 60, 120, and 240 min ($n = 6–7$). The value is normalized to the length of the artery. Statistical significance between $Fbln5^{+/+}$ and $Fbln5^{-/-}$ (*) was determined at the indicated dextran size and time. Error bars are SEM for clarity. Panel *c*—isolated results at 60 min including 150 kDa FITC-dextran and elastase-treated artery experiments. Statistical significance between $Fbln5^{+/+}$ and $Fbln5^{-/-}$ (*), $Fbln5^{+/+}$ and elastase-treated $Fbln5^{+/+}$ (†), and $Fbln5^{+/+}$ and elastase-treated $Fbln5^{+/+}$ (#) are indicated. Error bars are SD.

While there is no clear trend in hydraulic conductance with number of elastic lamellae from these literature values, the results from our study suggest the architecture of the elastic fiber network should be a determining factor. We propose that the hydraulic resistance of the arterial media is equivalent to the sum of the hydraulic resistances of each individual lamellae. Our hypothesis is only applicable if the elastic fiber component of the wall has a prominent effect on transport since without elastic fibers the wall would more closely resemble a homogenous tissue of VSMCs and other ECM constituents. Future investigation is needed to determine whether a relationship exists between hydraulic resistance and number of elastic lamellae. If such a relation exists, then it would be beneficial knowledge toward the design of drug delivery strategies. The drug concentration loaded onto the delivery platform may be adjusted according to the elastic fiber network structure of the targeted artery to improve the therapeutic response.

Elastic and collagen fiber arrangement and structure in the arterial wall are affected by physiological mechanical loading. Circumferential strain applied by increases in blood pressure results in the rearrangement and straightening of these ECM components [52,53]. Previous investigations indicate a dependence of arterial hydraulic conductance changes on the pressure gradient across the wall [45,46,48]. By our findings, it is reasonable to suggest that rearrangement of the ECM in response to changes in pressure is one of the mechanisms responsible for this dependence. The large arteries experience dynamic changes in acting forces, implicating that the intrinsic transport properties may be more dynamic than what is typically assumed.

Aortic aneurysms have severe structural defects in the arterial wall ECM microstructure including fragmentation and degradation of the elastic lamellae. The results from our study suggest that aneurysmal tissue could have increased hydraulic conductivity and effective porosity compared to surrounding healthy arterial tissue. One therapeutic strategy may be to design anti-inflammatory drug delivery systems which take advantage of this difference in transport properties. A delivery vehicle small enough to enter into the aneurysmal tissue from the arterial lumen but too large to diffuse to surrounding healthier tissue may effectively concentrate the drug to the diseased area.

Accumulation of defects to the elastic fiber network of arterial tissues is observed in aging and disease progression. Elastic fiber degradation is a factor in numerous cardiovascular diseases including hypertension, aneurysm development, and arterial calcification [54–57]. Reduced elastic fiber crosslinking, increased elastolytic activity, and higher elastic fiber fragmentation has been observed in mouse models of obesity [58]. Elastic fiber fragmentation may be involved in both the initiation of plaque development in atherosclerosis [59] and exacerbation of the disease [60–62]. In aging, elastic fiber composition in the large conduit arteries drops over the human lifespan [57,63], but this is likely an effect of disproportionate increases of other ECM constituents in the wall while changes to elastic fiber quantity is nominal [64,65]. Elastic fibers do, however, accumulate damage and defects over time resulting in increased fragmentation with aging [66], as de novo elastic fiber synthesis or repair is not evident in adult tissues [54]. The cause of fragmentation is not well understood but it is likely that the high number of cardiac loading cycles over an organism's lifetime causes mechanical failure in the elastic fiber network [67] for which there is no known repair mechanism. It is also thought that an imbalance in the elastolytic enzymes contributes to elastic fiber degradation [56,68]. The influence on arterial transport by elastic fiber integrity has important implications on the kinetics of biomolecules involved in aging and cardiovascular disease, warranting future investigation.

Similar to an aged artery, arteries from $Fbln5^{-/-}$ mice do not demonstrate appreciable changes in elastic fiber amount although they do not have the same increases in collagen content normally associated with aged arteries [32,69]. Fragmentation in arterial elastic lamellae of $Fbln5^{-/-}$ mice is a result of improper elastic fiber assembly in development rather than mechanical fatigue and

there is no evidence of heightened elastolytic activity [31,32,34]. As such, the disruption to the elastic fiber network in $Fbln5^{-/-}$ mouse occurs through a different mechanism than the damage that accumulates in the elastic fibers of aged human arteries. Regardless, in the context of transport the result is likely similar such that a similar decrease in resistance to advective mass transport that we report for $Fbln5^{-/-}$ carotids may also occur in aged arteries. Additionally, the experiments using an elastase treatment for elastic fiber degradation in most cases demonstrate similar results as the $Fbln5^{-/-}$ experiments providing evidence that elastic fiber degradation, regardless of the mechanism responsible, can largely impact transport. The degradation of an individual's arterial elastic fiber network in aging and disease could impact the transport of biomolecules and drugs across the arterial wall and has implications for the progression of vascular disease and efficacy of drug delivery therapies that target the arterial media.

Conclusions

We have investigated the transport properties of elastic fiber compromised arterial tissue to evaluate whether changes to the elastic fiber network structure have significant impact on the transport properties of the arterial wall. It is apparent from our histological cross section and en face two-photon microscopy images that $Fbln5^{-/-}$ carotids have several phenotypic changes to the structure of the elastic lamellae including a fragmented appearance. We hypothesized that these structural changes would translate to a decrease in tissue porosity and tested this hypothesis with measures of fluid and solute transport. We observed an increase in hydraulic conductance, net solute flux, and reduced solute uptake compared to $Fbln5^{+/+}$ carotids and conclude this to be strong evidence that the elastic fiber network plays a significant role in determining the transport properties of the arterial wall. Similar changes in most cases were observed when the elastic fiber network was exposed to a brief elastase treatment.

From our results, the native elastic fiber network within the arterial media contributes to the resistance of bulk transport across the arterial media. Elastic fibers predominately form sheet-like layers within the arterial wall and are partly responsible for the nonhomogenous structure of the media. Previous transport studies have approximated the media to be homogenous and have largely ignored the elastic fiber component. Our results suggest this may be an oversimplification that should be addressed in future studies to improve the understanding of transport within arterial tissue. Fragmentation, rearrangement, and degradation of the elastic fiber network in disease and aging may have significant impact on the transport of macromolecules within the arterial wall and could impact effectiveness of drug delivery therapies targeting these tissues.

Limitations

In this study, we made the assumption that diffusive solute transport was insignificant compared to advective transport. This is supported by several previous numerical and experimental investigations that have reported high Péclet numbers for small molecules and small proteins in arterial tissue [17,29,70,71]. However, we observed a steady increase in solute uptake within the tissue even after 4 h despite steady-state, transmural advective transport being achieved in less than 10 min. This is possibly a consequence of passive diffusion including diffusion in directions other than across the wall. This observation indicates that arterial wall transport from the lumen and across the wall is not sufficiently described in the one-dimensional scenario, especially since the nonhomogenous elastic fiber network has an impact on solute transport. Three-dimensional diffusion is difficult to measure given the small size of the mouse carotid tissue, especially if in vivo conformation is to be retained. However, our results provide new evidence for the contribution of the elastic fiber component to arterial wall transport to better inform more complex theoretical transport models.

Another limitation to this study is that concentration polarization may be a contributing factor toward the overall solute transport. Without measurements of changes in FITC-dextran concentration in the lumen throughout the course of the experiment, it is difficult to conclude to what degree concentration polarization affects the results of this study. However, the constant rate of solute transport for each FITC-dextran in Fig. 4 is evidence against concentration polarization having a significant affect in this study but may be an important in future studies.

Acknowledgment

Hiromi Yanagisawa at the University of Tsukuba is gratefully acknowledged for providing the $Fbln5^{-/-}$ mice. Data presented in this study were partially funded by NIH grants R01HL115560, R01HL105314, and T32EB018266. Histological data were partially provided by the Washington University Musculoskeletal Research Center funded by NIH grant P30 AR057235. Confocal data were generated on a Zeiss LSM 880 Airyscan Confocal Microscope which was purchased with support from the Office of Research Infrastructure Programs (ORIP), a part of the NIH Office of the Director under grant OD021629. The content is solely the responsibility of the authors and does not necessarily represent the official views of the NIH.

Funding Data

- National Heart, Lung, and Blood Institute (Grant Nos. R01HL105314 and R01HL115560, Funder ID. 10.13039/100000050).
- National Institute of Arthritis and Musculoskeletal and Skin Diseases (Grant No. P30AR057235, Funder ID. 10.13039/100000069).
- National Institute of Biomedical Imaging and Bioengineering (Grant No. T32EB018266, Funder ID. 10.13039/100000070).
- NIH Office of the Director (Grant No. OD021629, Funder ID. 10.13039/100000052).

References

[1] Pellegrini, D. O., Gomes, V. O., Lasevitch, R., Smidt, L., Azeredo, M. A., Ledur, P., Bodanese, R., Sinnott, L., Moriguchi, E., and Caramori, P., 2014, "Efficacy and Safety of Drug-Eluting Stents in the Real World: 8-Year Follow-Up," Arq. Bras. Cardiol., **103**(3), pp. 174–82.

[2] Buchanan, K., Steinvil, A., and Waksman, R., 2017, "Does the New Generation of Drug-Eluting Stents Render Bare Metal Stents Obsolete?," Cardiovasc. Revasc. Med., **18**(6), pp. 456–461.

[3] Cui, K., Lyu, S., Song, X., Yuan, F., Xu, F., Zhang, M., Wang, W., Zhang, D., and Dai, J., 2017, "Drug-Eluting Balloon Versus Bare-Mental Stent and Drug-Eluting Stent for De Novo Coronary Artery Disease: A Systematic Review and Meta-Analysis of 14 Randomized Controlled Trials," PLoS One, **12**(4), p. e0176365.

[4] Collins, M. J., Li, X., Lv, W., Yang, C., Protack, C. D., Muto, A., Jadlowiec, C. C., Shu, C., and Dardik, A., 2012, "Therapeutic Strategies to Combat Neointimal Hyperplasia in Vascular Grafts," Expert Rev. Cardiovasc. Ther., **10**(5), pp. 635–647.

[5] Seedial, S. M., Ghosh, S., Saunders, R. S., Suwanabol, P. A., Shi, X., Liu, B., and Kent, K. C., 2013, "Local Drug Delivery to Prevent Restenosis," J. Vasc. Surg., **57**(5), pp. 1403–1414.

[6] Golledge, J., Cullen, B., Moran, C., and Rush, C., 2010, "Efficacy of Simvastatin in Reducing Aortic Dilatation in Mouse Models of Abdominal Aortic Aneurysm," Cardiovasc. Drugs Ther., **24**(5–6), pp. 373–378.

[7] Steinmetz, E. F., Buckley, C., Shames, M. L., Ennis, T. L., Vanvickle-Chavez, S. J., Mao, D., Goeddel, L. A., Hawkins, C. J., and Thompson, R. W., 2005, "Treatment With Simvastatin Suppresses the Development of Experimental Abdominal Aortic Aneurysms in Normal and Hypercholesterolemic Mice," Ann. Surg., **241**(1), pp. 92–101.

[8] Moore, G., Liao, S., Curci, J. A., Starcher, B. C., Martin, R. L., Hendricks, R. T., Chen, J. J., and Thompson, R. W., 1999, "Suppression of Experimental Abdominal Aortic Aneurysms by Systemic Treatment With a Hydroxamate-Based Matrix Metalloproteinase Inhibitor (RS 132908)," J. Vasc. Surg., **29**(3), pp. 522–532.

[9] Fraga-Silva, R. A., Trachet, B., and Stergiopulos, N., 2015, "Emerging Pharmacological Treatments to Prevent Abdominal Aortic Aneurysm Growth and Rupture," Curr. Pharm. Des., **21**(28), pp. 4000–4006.

[10] Kurosawa, K., Matsumura, J. S., and Yamanouchi, D., 2013, "Current Status of Medical Treatment for Abdominal Aortic Aneurysm," Circ. J., **77**(12), pp. 2860–2866.

[11] Yoshimura, K., Morikage, N., Nishino-Fujimoto, S., Furutani, A., Shirasawa, B., and Hamano, K., 2017, "Current Status and Perspectives on Pharmacologic

Therapy for Abdominal Aortic Aneurysm," Curr Drug Targets, **19**(11), pp. 1265–1275.
[12] Shirasu, T., Koyama, H., Miura, Y., Hoshina, K., Kataoka, K., and Watanabe, T., 2016, "Nanoparticles Effectively Target Rapamycin Delivery to Sites of Experimental Aortic Aneurysm in Rats," PLoS One, **11**(6), p. e0157813.
[13] Nosoudi, N., Chowdhury, A., Siclari, S., Parasaram, V., Karamched, S., and Vyavahare, N., 2016, "Systemic Delivery of Nanoparticles Loaded With Pentagalloyl Glucose Protects Elastic Lamina and Prevents Abdominal Aortic Aneurysm in Rats," J. Cardiovasc. Transl. Res., **9**(5–6), pp. 445–455.
[14] Wang, X., Searle, A. K., Hohmann, J. D., Liu, A. L., Abraham, M. K., Palasubramaniam, J., Lim, B., Yao, Y., Wallert, M., Yu, E., Chen, Y. C., and Peter, K., 2018, "Dual-Targeted Theranostic Delivery of miRs Arrests Abdominal Aortic Aneurysm Development," Mol. Ther., **26**(4), pp. 1056–1065.
[15] Nosoudi, N., Nahar-Gohad, P., Sinha, A., Chowdhury, A., Gerard, P., Carsten, C. G., Gray, B. H., and Vyavahare, N. R., 2015, "Prevention of Abdominal Aortic Aneurysm Progression by Targeted Inhibition of Matrix Metalloproteinase Activity With Batimastat-Loaded Nanoparticles," Circ. Res., **117**(11), pp. e80–e89.
[16] Sivaraman, B., and Ramamurthi, A., 2013, "Multifunctional Nanoparticles for Doxycycline Delivery Towards Localized Elastic Matrix Stabilization and Regenerative Repair," Acta Biomater., **9**(5), pp. 6511–6525.
[17] Hwang, C. W., Wu, D., and Edelman, E. R., 2001, "Physiological Transport Forces Govern Drug Distribution for Stent-Based Delivery," Circulation, **104**(5), pp. 600–605.
[18] Davis, E. C., 1993, "Stability of Elastin in the Developing Mouse Aorta: A Quantitative Radioautographic Study," Histochemistry, **100**(1), pp. 17–26.
[19] Dingemans, K. P., Teeling, P., Lagendijk, J. H., and Becker, A. E., 2000, "Extracellular Matrix of the Human Aortic Media: An Ultrastructural Histochemical and Immunohistochemical Study of the Adult Aortic Media," Anat. Rec., **258**(1), pp. 1–14.
[20] O'Connell, M. K., Murthy, S., Phan, S., Xu, C., Buchanan, J., Spilker, R., Dalman, R. L., Zarins, C. K., Denk, W., and Taylor, C. A., 2008, "The Three-Dimensional Micro- and Nanostructure of the Aortic Medial Lamellar Unit Measured Using 3D Confocal and Electron Microscopy Imaging," Matrix Biol., **27**(3), pp. 171–181.
[21] Ramirez, C. A., Colton, C. K., Smith, K. A., Stemerman, M. B., and Lees, R. S., 1984, "Transport of 125I-Albumin Across Normal and Deendothelialized Rabbit Thoracic Aorta In Vivo," Aeteriosclerosis, **4**(3), pp. 283–291.
[22] Caro, C. G., Lever, M. J., Laver-Rudich, Z., Meyer, F., Liron, N., Ebel, W., Parker, K. H., and Winlove, C. P., 1980, "Net Albumin Transport Across the Wall of the Rabbit Common Carotid Artery Perfused In Situ," Atherosclerosis, **37**(4), pp. 497–511.
[23] Pfeffer, R., Ganatos, P., Nir, A., and Weinbaum, S., 1981, "Diffusion of Macromolecules Across the Arterial Wall in the Presence of Multiple Endothelial Injuries," ASME J. Biomech. Eng., **103**(3), pp. 197–203.
[24] Proctor, S. D., Vine, D. F., and Mamo, J. C., 2004, "Arterial Permeability and Efflux of Apolipoprotein B-Containing Lipoproteins Assessed by in Situ Perfusion and Three-Dimensional Quantitative Confocal Microscopy," Arterioscler. Thromb. Vasc. Biol., **24**(11), pp. 2162–2167.
[25] Tada, S., and Tarbell, J. M., 2004, "Internal Elastic Lamina Affects the Distribution of Macromolecules in the Arterial Wall: A Computational Study," Am. J. Physiol. Heart Circ. Physiol., **287**(2), pp. H905–H913.
[26] Huang, Z. J., and Tarbell, J. M., 1997, "Numerical Simulation of Mass Transfer in Porous Media of Blood Vessel Walls," Am. J. Physiol., **273**(1), pp. H464–H477.
[27] Fry, D. L., 1985, "Mathematical Models of Arterial Transmural Transport," Am. J. Physiol., **248**(2), pp. H240–H263.
[28] Caro, C. G., and Lever, M. J., 1984, "Factors Influencing Arterial Wall Mass Transport," Biorheology, **21**(1–2), pp. 197–205.
[29] Kim, W. S., and Tarbell, J. M., 1994, "Macromolecular Transport Through the Deformable Porous Media of an Artery Wall," ASME J. Biomech. Eng., **116**(2), pp. 156–163.
[30] Hwang, C. W., and Edelman, E. R., 2002, "Arterial Ultrastructure Influences Transport of Locally Delivered Drugs," Circ. Res., **90**(7), pp. 826–832.
[31] Nakamura, T., Lozano, P. R., Ikeda, Y., Iwanaga, Y., Hinek, A., Minamisawa, S., Cheng, C. F., Kobuke, K., Dalton, N., Takada, Y., Tashiro, K., Ross, J., Jr., Honjo, T., and Chien, K. R., 2002, "Fibulin-5/DANCE is Essential for Elastogenesis In Vivo," Nature, **415**(6868), pp. 171–175.
[32] Le, V. P., Cheng, J. K., Kim, J., Staiculescu, M. C., Ficker, S. W., Sheth, S. C., Bhayani, S. A., Mecham, R. P., Yanagisawa, H., and Wagenseil, J. E., 2015, "Mechanical Factors Direct Mouse Aortic Remodelling During Early Maturation," J. R. Soc., Interface, **12**(104), p. 20141350.
[33] Kedem, O., and Katchalsky, A., 1958, "Thermodynamic Analysis of the Permeability of Biological Membranes to Non-Electrolytes," Biochim. Biophys. Acta., **27**(2), pp. 229–246.
[34] Yanagisawa, H., Davis, E. C., Starcher, B. C., Ouchi, T., Yanagisawa, M., Richardson, J. A., and Olson, E. N., 2002, "Fibulin-5 is an Elastin-Binding Protein Essential for Elastic Fibre Development In Vivo," Nature, **415**(6868), pp. 168–171.
[35] Ferruzzi, J., Bersi, M. R., Uman, S., Yanagisawa, H., and Humphrey, J. D., 2015, "Decreased Elastic Energy Storage, Not Increased Material Stiffness, Characterizes Central Artery Dysfunction in Fibulin-5 Deficiency Independent of Sex," ASME J. Biomech. Eng., **137**(3), p. 031007.
[36] Luetkemeyer, C. M., James, R. H., Devarakonda, S. T., Le, V. P., Liu, Q., Han, H. C., and Wagenseil, J. E., 2015, "Critical Buckling Pressure in Mouse Carotid Arteries With Altered Elastic Fibers," J. Mech. Behav. Biomed. Mater., **46**, pp. 69–82.
[37] Ralevic, V., Kristek, F., Hudlicka, O., and Burnstock, G., 1989, "A New Protocol for Removal of the Endothelium From the Perfused Rat Hind-Limb Preparation," Circ. Res., **64**(6), pp. 1190–1196.
[38] Winkler, R. H., 1978, "The Effect of Halides (NaCl and NaI) on In Vitro Pancreatic Elastase Activity," Connect. Tissue Res., **6**(2), pp. 89–92.
[39] Wan, W., Yanagisawa, H., and Gleason, R. L., Jr., 2010, "Biomechanical and Microstructural Properties of Common Carotid Arteries From Fibulin-5 Null Mice," Ann. Biomed. Eng., **38**(12), pp. 3605–3617.
[40] Wong, L. C., and Langille, B. L., 1996, "Developmental Remodeling of the Internal Elastic Lamina of Rabbit Arteries: Effect of Blood Flow," Circ. Res., **78**(5), pp. 799–805.
[41] Armstrong, J. K., Wenby, R. B., Meiselman, H. J., and Fisher, T. C., 2004, "The Hydrodynamic Radii of Macromolecules and Their Effect on Red Blood Cell Aggregation," Biophys. J., **87**(6), pp. 4259–70.
[42] Lopez-Guimet, J., Andilla, J., Loza-Alvarez, P., and Egea, G., 2017, "High-Resolution Morphological Approach to Analyse Elastic Laminae Injuries of the Ascending Aorta in a Murine Model of Marfan Syndrome," Sci. Rep., **7**(1), p. 1505.
[43] Ushiki, T., 2002, "Collagen Fibers, Reticular Fibers and Elastic Fibers. A Comprehensive Understanding From a Morphological Viewpoint," Arch. Histol. Cytol., **65**(2), pp. 109–126.
[44] Tedgui, A., and Lever, M. J., 1984, "Filtration Through Damaged and Undamaged Rabbit Thoracic Aorta," Am. J. Physiol., **247**(5), pp. H784–H791.
[45] Baldwin, A. L., and Wilson, L. M., 1993, "Endothelium Increases Medial Hydraulic Conductance of Aorta, Possibly by Release of EDRF," Am. J. Physiol., **264**(1), pp. H26–H32.
[46] Shou, Y., Jan, K. M., and Rumschitzki, D. S., 2006, "Transport in Rat Vessel Walls—I: Hydraulic Conductivities of the Aorta, Pulmonary Artery, and Inferior Vena Cava With Intact and Denuded Endothelia," Am. J. Physiol. Heart Circ. Physiol., **291**(6), pp. H2758–H2771.
[47] Wolinsky, H., and Glagov, S., 1967, "A Lamellar Unit of Aortic Medial Structure and Function in Mammals," Circ. Res., **20**(1), pp. 99–111.
[48] Baldwin, A. L., Wilson, L. M., and Simon, B. R., 1992, "Effect of Pressure on Aortic Hydraulic Conductance," Arterioscler. Thromb., **12**(2), pp. 163–171.
[49] Tarbell, J. M., Lever, M. J., and Caro, C. G., 1988, "The Effect of Varying Albumin Concentration of the Hydraulic Conductivity of the Rabbit Common Carotid Artery," Microvasc. Res., **35**(2), pp. 204–220.
[50] Williams, C., Liao, J., Joyce, E. M., Wang, B., Leach, J. B., Sacks, M. S., and Wong, J. Y., 2009, "Altered Structural and Mechanical Properties in Decellularized Rabbit Carotid Arteries," Acta Biomater., **5**(4), pp. 993–1005.
[51] Rees, P. M., 1968, "Electron Microscopical Observations on the Architecture of the Carotid Arterial Walls, With Special Reference to the Sinus Portion," J. Anat., **103**(Pt. 1), pp. 35–47.
[52] Sugita, S., and Matsumoto, T., 2017, "Multiphoton Microscopy Observations of 3D Elastin and Collagen Fiber Microstructure Changes During Pressurization in Aortic Media," Biomech. Model. Mechanobiol., **16**(3), pp. 763–773.
[53] Chow, M. J., Turcotte, R., Lin, C. P., and Zhang, Y., 2014, "Arterial Extracellular Matrix: A Mechanobiological Study of the Contributions and Interactions of Elastin and Collagen," Biophys. J., **106**(12), pp. 2684–2692.
[54] Cocciolone, A. J., Hawes, J. Z., Staiculescu, M. C., Johnson, E. O., Murshed, M., and Wagenseil, J. E., 2018, "Elastin, Arterial Mechanics, and Cardiovascular Disease," Am. J. Physiol. Heart Circ. Physiol., **315**(2), pp. H189–H205.
[55] Baldwin, A. K., Simpson, A., Steer, R., Cain, S. A., and Kielty, C. M., 2013, "Elastic Fibres in Health and Disease," Expert Rev. Mol. Med., **15**, p. e8.
[56] Duca, L., Blaise, S., Romier, B., Laffargue, M., Gayral, S., El Btaouri, H., Kawecki, C., Guillot, A., Martiny, L., Debelle, L., and Maurice, P., 2016, "Matrix Ageing and Vascular Impacts: Focus on Elastin Fragmentation," Cardiovasc. Res., **110**(3), pp. 298–308.
[57] Tsamis, A., Krawiec, J. T., and Vorp, D. A., 2013, "Elastin and Collagen Fibre Microstructure of the Human Aorta in Ageing and Disease: A Review," J. R. Soc., Interface, **10**(83), p. 20121004.
[58] Chen, J. Y., Tsai, P. J., Tai, H. C., Tsai, R. L., Chang, Y. T., Wang, M. C., Chiou, Y. W., Yeh, M. L., Tang, M. J., Lam, C. F., Shiesh, S. C., Li, Y. H., Tsai, W. C., Chou, C. H., Lin, L. J., Wu, H. L., and Tsai, Y. S., 2013, "Increased Aortic Stiffness and Attenuated Lysyl Oxidase Activity in Obesity," Arterioscler. Thromb. Vasc. Biol., **33**(4), pp. 839–846.
[59] Akima, T., Nakanishi, K., Suzuki, K., Katayama, M., Ohsuzu, F., and Kawai, T., 2009, "Soluble Elastin Decreases in the Progress of Atheroma Formation in Human Aorta," Circ. J., **73**(11), pp. 2154–2162.
[60] Van der Donckt, C., Van Herck, J. L., Schrijvers, D. M., Vanhoutte, G., Verhoye, M., Blockx, I., Van Der Linden, A., Bauters, D., Lijnen, H. R., Sluimer, J. C., Roth, L., Van Hove, C. E., Fransen, P., Knaapen, M. W., Hervent, A. S., De Keulenaer, G. W., Bult, H., Martinet, W., Herman, A. G., and De Meyer, G. R., 2015, "Elastin Fragmentation in Atherosclerotic Mice Leads to Intraplaque Neovascularization, Plaque Rupture, Myocardial Infarction, Stroke, and Sudden Death," Eur. Heart J., **36**(17), pp. 1049–1058.
[61] Maedeker, J. A., Stoka, K. V., Bhayani, S. A., Gardner, W. S., Bennett, L., Procknow, J. D., Staiculescu, M. C., Walji, T. A., Craft, C. S., and Wagenseil, J. E., 2016, "Hypertension and Decreased Aortic Compliance Due to Reduced Elastin Amounts Do Not Increase Atherosclerotic Plaque Accumulation in Ldlr−/− Mice," Atherosclerosis, **249**, pp. 22–29.
[62] Stoka, K. V., Maedeker, J. A., Bennett, L., Bhayani, S. A., Gardner, W. S., Procknow, J. D., Cocciolone, A. J., Walji, T. A., Craft, C. S., and Wagenseil, J. E., 2018, "Effects of Increased Arterial Stiffness on Atherosclerotic Plaque Amounts," ASME J. Biomech. Eng., **140**(5), p. 051007.
[63] Hosoda, Y., Kawano, K., Yamasawa, F., Ishii, T., Shibata, T., and Inayama, S., 1984, "Age-Dependent Changes of Collagen and Elastin Content in Human Aorta and Pulmonary Artery," Angiology, **35**(10), pp. 615–621.

[64] Spina, M., Garbisa, S., Hinnie, J., Hunter, J. C., and Serafini-Fracassini, A., 1983, "Age-Related Changes in Composition and Mechanical Properties of the Tunica Media of the Upper Thoracic Human Aorta," Aeteriosclerosis, **3**(1), pp. 64–76.
[65] Fritze, O., Romero, B., Schleicher, M., Jacob, M. P., Oh, D. Y., Starcher, B., Schenke-Layland, K., Bujan, J., and Stock, U. A., 2012, "Age-Related Changes in the Elastic Tissue of the Human Aorta," J. Vasc. Res., **49**(1), pp. 77–86.
[66] Sans, M., and Moragas, A., 1993, "Mathematical Morphologic Analysis of the Aortic Medial Structure. Biomechanical Implications," Anal. Quant. Cytol. Histol., **15**(2), pp. 93–100.
[67] Avolio, A., Jones, D., and Tafazzoli-Shadpour, M., 1998, "Quantification of Alterations in Structure and Function of Elastin in the Arterial Media," Hypertension, **32**(1), pp. 170–175.
[68] Wang, M., and Lakatta, E. G., 2002, "Altered Regulation of Matrix Metalloproteinase-2 in Aortic Remodeling During Aging," Hypertension, **39**(4), pp. 865–873.
[69] Wan, W., and Gleason, R. L., Jr., 2013, "Dysfunction in Elastic Fiber Formation in Fibulin-5 Null Mice Abrogates the Evolution in Mechanical Response of Carotid Arteries During Maturation," Am. J. Physiol. Heart Circ. Physiol., **304**(5), pp. H674–H686.
[70] Baldwin, A. L., Wilson, L. M., Gradus-Pizlo, I., Wilensky, R., and March, K., 1997, "Effect of Atherosclerosis on Transmural Convection an Arterial Ultrastructure. Implications Local Intravascular Drug Delivery," Arterioscler. Thromb. Vasc. Biol., **17**(12), pp. 3365–3375.
[71] Tedgui, A., and Lever, M. J., 1985, "The Interaction of Convection and Diffusion in the Transport of 131I-Albumin Within the Media of the Rabbit Thoracic Aorta," Circ. Res., **57**(6), pp. 856–863.